PAPER • OPEN ACCESS

Dynamic characteristics of edge plasma profiles during the opening of edge islands on the J-TEXT tokamak

Dynamic characteristics of edge plasma profiles during the opening of edge islands on the J-TEXT tokamak

J. Yang[1,2]**, Y. Liang**[1,2,4,*] **, P. Shi**[3]**, N.C. Wang**[1] **, S. Zhou**[1] **, Z.P. Chen**[1] **, Z.H. Jiang**[1] **, F.Y. Mao**[1]**, Q.H. Yang**[1]**, J.K. Hua**[1]**, D. Li**[1]**, Z.Y. Chen**[1] **, Y.H. Ding**[1]**, P. Drews**[2] **, A. Knieps**[2] **, E. Wang**[2]**, S. Xu**[2] **, H.M. Xiang**[2]**, J.Q. Cai**[2]**, J. Huang**[2]**, Y.C. Gao**[2]**, J.W. Liu**[2,4] **, Y. Luo**[2]**, L. Liao**[2,4] **and the J-TEXT team**[1,a]

[1] State Key Laboratory of Advanced Electromagnetic Engineering and Technology, International Joint Research Laboratory of Magnetic Confinement Fusion and Plasma Physics, School of Electrical and Electronic Engineering, Huazhong University of Science and Technology, Wuhan 430074, China
[2] Forschungszentrum Jülich GmbH, Institut für Energie- und Klimaforschung—Plasmaphysik, Partner of the Trilateral Euregio Cluster (TEC), 52425 Jülich, Germany
[3] United Kingdom Atomic Energy Authority, Culham Centre for Fusion Energy, Culham Science Centre, Abingdon, Oxon OX14 3 DB, United Kingdom of Great Britain and Northern Ireland
[4] Institute of Plasma Physics, Chinese Academy of Sciences, Hefei 230031, China

E-mail: y.liang@fz-juelich.de

CrossMark

Abstract

On the J-TEXT tokamak, the dynamics of edge magnetic topology during the opening of the edge magnetic islands induced by the external Resonant Magnetic Perturbation (RMP) are investigated. The edge island chain is pushed outward by increasing plasma toroidal current to intersect the poloidally and toroidally localized divertor plate, forming an open magnetic island in the Scrape-Off Layer (SOL). The location of the strike points on the divertor plate predicted by the HINT code is in agreement with the experimental observations. The influence of the magnetic topology on edge plasma profiles has also been investigated using Langmuir probes. The properties of edge T_e, n_e, P_e and E_r profiles are studied as function of three magnetic structures in q_a-dependence experiments and two magnetic structures in RMP configuration-dependence experiments. Some common features are observed. Inside the edge closed and SOL remnant islands, flat P_e but non-flat T_e and n_e profiles are detected. When transitioning from the edge closed island to the partially open island with remnant island, the local flat P_e profile is shifted outward accompanied by a narrower flattened P_e region. The steep slopes of T_e, n_e and P_e are measured in the SOL regions characterized by a long connection length L_c, and the longer L_c, the steeper slopes. E_r exhibits a negative well inside the remnant island with infinite L_c and in the SOL regions where L_c significantly exceeds than the electron mean free path λ_e, but develops a positive value in the SOL regions where L_c is relatively short.

1. Introduction

For the future fusion reactors such as ITER, one of the key challenges is to efficiently control heat and particle exhausts to the tolerable levels. In this context, it is of great significance to explore the plasma transport physics at the plasma edge, divertor and the Scrape-Off Layer (SOL).

Three-Dimensional (3D) magnetic topologies have been introduced in tokamak plasmas for a wide range of applications, such as the optimization of magnetic configuration [1] and the mitigation of Edge Localized Modes (ELMs) [2]. They have also been demonstrated to effectively control the transport of heat and particles [3, 4]. The magnetic island and stochastic zone are the two fundamental 3D structures of magnetic field. Magnetic islands, structures that break the nested magnetic flux surfaces of fusion plasma, are known to flatten the local plasma temperature and pressure profiles in the absence of the heat source since the parallel transport along the reconnected field lines on either side of island O-point becomes dominant over the perpendicular transport [5–9]. Additionally, magnetic islands can trigger the formation of transport barriers due to the strong poloidal flow shear generated near the island separatrix [10, 11]. When two or more nearby magnetic island chains grow to the point where they overlap, stochastic magnetic fields can form due to the destruction of magnetic flux surfaces between them. The stochastic magnetic field layer at the plasma boundary plays a critical role in optimizing the plasma-wall interaction on many devices, such as TEXTOR [12], DIII-D [13] and TEXT [14]. Experimental results have also shown that the stochastization can strongly modify the edge temperature, density profiles as well as radial electric field [15–19]. Furthermore, resonant magnetic perturbation (RMP) is one of the options for the control of large type-I ELMs for ITER. The application of RMP leads to 3D pattern of edge transport and plasma-wall interaction [20]. Therefore, a thorough comprehension of transport in 3D magnetic topology is crucial for the ITER project.

On the J-TEXT tokamak, many efforts have been devoted to studying plasma responses to RMP, such as electron density transport with $m/n = 3/1$ RMP [21], the plasma penetration of $m/n = 2/1$ RMP [22] and the plasma rotation response to $m/n = 2/1$ RMP [23]. In these previous works, the closed magnetic islands inside the Last Closed Flux Surface (LCFS) are emphasized. Here, m and n are the poloidal and toroidal mode numbers, respectively. In [24]., the carbon impurity screening effect shows a dependence on the phase of the edge $m/n = 3/1$ magnetic island, which is considered to be contributed by the interaction between the edge island and limiter. In this paper, the dynamics of the edge plasma equilibrium profiles on J-TEXT during the opening of the edge $m/n = 3/1$ magnetic island generated by the RMP are experimental observed for the

first time. The remainder of this paper is organized as follows: the experimental setup is described in section 2; the interaction between the edge islands and the poloidally localized limiter is discussed in section 3; the edge plasma profiles and island dynamics during the opening of edge island are presented in section 4. Finally, the discussion and conclusion are given in section 5.

2. Experimental setup

J-TEXT is a conventional medium-sized tokamak with a major radius of $R_0 = 1.05$ m and minor radius of $a = 0.25–0.29$ m [25]. There are four titanium-carbide-coated graphite rail limiters, one of which is fixed at the High Field Side (HFS) with a toroidal angle of $\phi_{\rm tor} = 247.5°$, a width of 0.058 m in the toroidal direction and a minor radii of 0.265 m from the center of the vacuum chamber; and the other three are movable and located in different poloidal positions (top, middle at the Low Field Side (LFS) and bottom) at $\phi_{\rm tor} = 337.5°$ with a width of 0.050 m in the toroidal direction. In this experiment, these three movable limiters are placed at the minor radii of 0.275 m, 0.255 m, and 0.255 m, respectively. The parameters in ohmic hydrogen discharge for this experiment are: plasma current $I_{\rm p} = 150 - 180$kA, toroidal magnetic field $B_{\rm t} = 1.4$T, the central line-averaged electron density $n_{\rm e} = (1.2 - 1.4) \times 10^{19}$ m^{-3} and the edge safety factor is $q_{\rm a} = 2.7 - 3.4$.

As shown in figure 1(*a*), two sets of in-vessel RMP systems are constructed along the torus, consisting of 24 saddle coils situated at 8 toroidal locations and 3 poloidal locations (top, middle at LFS and bottom) [26, 27]. The red coil set is the double-turn type, while the blue coil set is the single-turn type. In this experiment, the top and bottom coils are employed to produce a static RMP with a large $m/n = 3/1$ resonant component. The spectrum of the RMPs, calculated without taking plasma responses into account (in vacuum conditions), is depicted in figure 1(*b*), where the $m/n = 3/1$ component at the plasma edge is $B_{\rm r}^{3/1} = 2.58$ Gs/kA ($\sim 7.4 \times 10^{-4}$ of $B_{\rm t}$ in the case of RMP current $I_{\rm RMP} = 4$kA). Two RMP configurations are performed by altering the polarity of the RMP coil current, as summarized in the second column of the table 1, where the symbol '+ (−)' denotes an outward- (inward-) pointing $B_{\rm r}$. The corresponding Poincaré plots, calculated with $I_{\rm p} = 160$kA ($q_{\rm a} = 3.2$) by the 3D non-linear Magnetohydrodynamical (MHD) equilibrium code HINT [28], of the plasma cross-section $\phi_{\rm tor} = 337.5°$ are shown in figures 1(*c*) and (*d*). In the first RMP configuration, the O-point of $m/n = 3/1$ magnetic island faces the bottom limiter. While in the second RMP configuration, the O-point faces the LFS limiter with a poloidal shift towards the bottom side. Due to the different poloidal positions of magnetic islands, different intersection patterns occur between the edge magnetic islands

Figure 1. (*a*) Layout of the RMP coils in J-TEXT, and the position of the reciprocating Langmuir probe. (*b*) 2D Fourier (*m, n*) spectrum of the radial magnetic field B_r generated by RMP coils at the plasma edge. (*c*)–(*d*) Poincaré plots of the plasma cross-section $\phi_{tor} = 337.5°$ for first and second RMP configurations, with three limiters at $\phi_{tor} = 337.5°$ indicated by black rectangles. The real parameter settings used in the prediction of magnetic topology are from discharges 1056901 and 1056898.

Table 1. Summarization of the RMP coil setup and plasma parameters implemented in the experiment.

Configuration	Polarity of RMP coils								Discharge	I_{RMP} (kA)	I_p (kA)	q_a
First	—	+	+	+	+	—	—	—	1056 894	4	150	3.4
	+	—	—	—	—	0	+	+	1056 901		160	3.2
									1056 903	3	180	2.8
Second	+	—	—	—	—	+	+	+	1056 898	4	160	3.2
	—	+	+	+	+	0	—	—	1056 905	3	150–180	3.4–2.8

Figure 2. The schematic layout of (*a*) Limiter Langmuir Probe Array (LLPA) and (*b*) Reciprocating Langmuir Probe (RLP).

and the poloidally localized limiters for the two configurations when the island is pushed outward. Furthermore, for the second RMP configuration, the stochastization around the boundary island is enhanced, which is due to the high-order modes generated by the missing coil at the bottom side of port 10.

Figure 2(*a*) shows the schematic layout of the Limiter Langmuir Probe Array (LLPA) [29], in which three movable limiters are mounted with nine tips and the fixed limiter is equipped with 21 tips. The tips are distributed symmetrically concerning the geometrical axis, with a distance of 25 mm between them. In this experiment, they are used to record the

floating potential V_f which is highly sensitive to the changes in the plasma footprint due to the modification of the magnetic topology. To address the boundary characterization during the opening of the edge magnetic island, the Reciprocating Langmuir Probe (RLP) mounted at the top window of the toroidal position $\phi_{tor} = 292.5°$ is employed to measure the edge profiles of electron temperature T_e, density n_e, pressure $P_e = T_e n_e$, floating potential V_f and radial electric field $E_r = -dV_f/dr - 2.5dT_e/dr$. In this paper, $E_r > 0$ (< 0) indicates a radially outside (inside) electric field. Figure 2(*b*) shows the schematic drawing of the tips of the RLP. Tip 5–8 are arranged as a standard four-tip triple probe, where tip 6 and tip 8 measure V_{f1} and V_{f2}, tip 5 and tip 7 are connected through a biasing voltage of 220 V to measure the positive potential of a double probe V_+ and ion saturation current I_s. The electron temperature and density are derived as $T_e = (V_+ - (V_{f1} + V_{f2})/2)/\ln 2$ and $n_e = I_s/(0.49 A_{eff} e c_s)$. A_{eff} is the effective probe surface area and $c_s = (k_B (Z_i T_e + T_i)/m_i)^{1/2}$ is the ion sound speed. Z_i is 1 for hydrogen plasma.

3. Interactions between the edge islands and the poloidally localized limiter

Figure 3 shows the time evolution of the plasma response during the opening of the edge $m/n = 3/1$ magnetic island in the discharge 1056905 with the second RMP configuration. The RMP coil current I_{RMP} is applied at $t = 0.21$ s and rumps up to the flattop of 3 kA at about $t = 0.25$ s (figure 3(*b*)). Field penetration occurs at $t = 0.255$ s, indicated by the rapidly increase of radial magnetic field B_r measured by the locked mode detectors. At this moment, the edge $m/n = 3/1$ magnetic island is formed, leading to a sharp drop in edge electron temperature T_e and the density-normalized carbon V (CV/n_e) radiation intensity and an increase in the density-normalized carbon III (CIII/n_e) radiation intensity, as shown in figures 3(*c*) and (*d*). Here, T_e is measured at $r = 23$ cm by using the Electron Cyclotron Emission (ECE) diagnostic [30] and the carbon impurities are measured by a spectral diagnostic system consisting of CV and CIII diagnostics [31]. The limiter ground current decreases at the LFS (I_{LFS}) and increases at the bottom side (I_{bottom}), respectively, as shown in figure 3(*e*). These observations of both the field penetration threshold and the effect of edge islands on impurity screening are consistent with previous studies on J-TEXT [21, 24]. As I_p increases and q_a decreases, the edge $m/n = 3/1$ magnetic island gradually shifts outward. It intersects with the poloidally localized limiter at around $t = 0.27$ s, and is progressively cut by the limiter over time. Correspondingly, the edge parameters also dynamically evolve with the change of the edge magnetic topology. CIII/n_e and CV/n_e radiation intensities begin to gradually decrease and increase, respectively. This result indicates that the impurity screening effect has a dependence on q_a (changes in magnetic topology). This issue is, however, beyond the scope of this paper and will be discussed elsewhere. The same experiment is also performed with the first RMP configuration, and
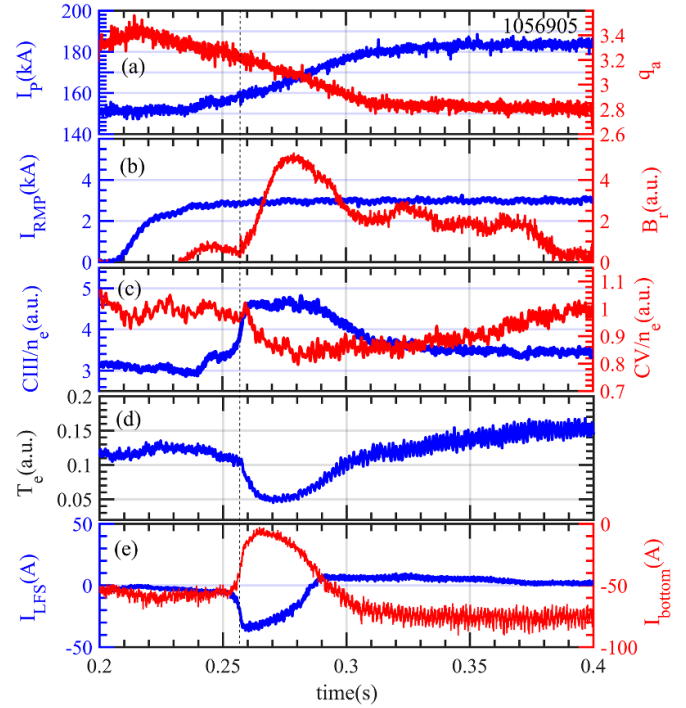

Figure 3. Time evolution of parameters for the discharge 1056 905 with $m/n = 3/1$ RMP, RMP penetration occurs at $t = 0.255$ s indicated by a dotted line. (*a*) Plasma toroidal current I_p and edge safety factor q_a, (*b*) RMP current I_{RMP} and radial magnetic field B_r, (*c*) density-normalized carbon III (CIII/n_e) and carbon V (CV/n_e) radiation intensity, (*d*) edge electron temperature T_e measured by ECE and (*e*) LFS and bottom limiter current I_{LFS} and I_{bottom}.

the plasma response to field penetration, impurity screening effect and parameter evolution during q_a reduction are very similar.

More experimental evidence of the intersection between edge island and limiter is given by the floating potentials V_f measured by LLPA, as depicted in figure 4. This figure plots the time evolution of V_f distribution along the limiter tiles for the corresponding discharge in figure 3. V_f is defined as the bias voltage where the probe draws no net current and is determined by the balance of electron and ion current to and from the probe [32]. The large negative V_f appear at the center of the bottom before RMP penetration, and switch to the center of the LFS at $t = 0.255$ s. This rapid transition is a result of the variation of the edge magnetic topology, i.e. the excitation of the edge $m/n = 3/1$ magnetic island and the O-point faces the LFS limiter (see figure 1(*d*)). As q_a decreases, the negative V_f distribution splits to two separate regions at $t \sim 0.27$ s on the LFS limiter. At $t \sim 0.3$ s, the peak position of the negative V_f distribution changes back to the center of the bottom.

To gain more insight into the V_f pattern during the q_a drop, the location of the strike points on the LFS limiter has been simulated by a field line tracing code. Here, the 3D plasma equilibrium perturbed by the $m/n = 3/1$ RMP was calculated using the HINT code. The strike points are formed by the intersection of the edge magnetic island with the LFS limiter target
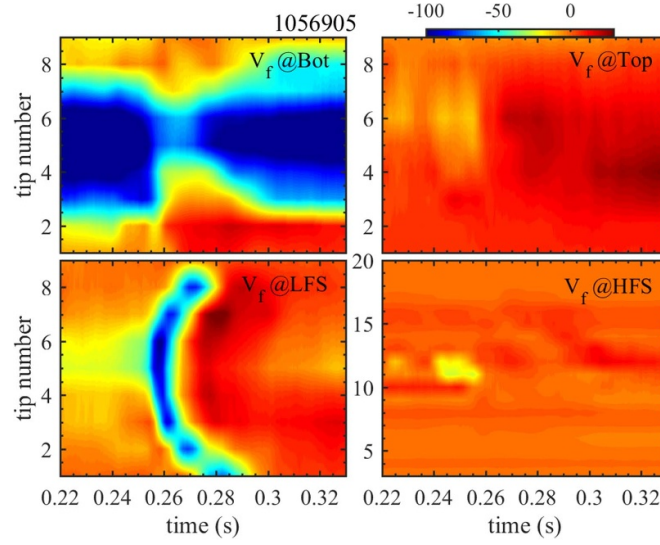
Figure 4. Time evolution of floating potential distribution measured by LLPA along the limiter tiles. The tip number of the vertical axis is indicated in the left plot of figure 2.
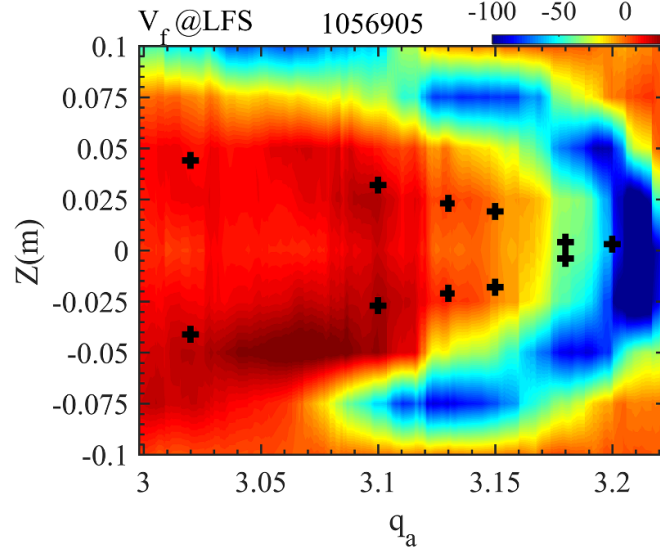

Figure 5. Dependence of LFS floating potential distribution on edge safety factor q_a. The black crosses are the strike points obtained from the field lines with the deepest penetration into the core plasma calculated by the field line tracing.

plate. By tracing the field lines from the LFS limiter into the SOL or core plasma, the location of the strike points can be determined from the peak of the minimum normalized poloidal magnetic flux $|\psi|_{min}$ distribution, so called the penetration depth [33]. A smaller $|\psi|_{min}$ represents a deeper penetration of the field line into the core plasma and $|\psi|_{min} = 1$ corresponds to the radial position of the original LCFS. Figure 5 shows the V_f profile and location of the strike points (black crosses) on the LFS limiter as a function of q_a. As q_a decreases from 3.2 to close to 3, the distance between two strike points continues to increase. The measured peak position of the negative V_f profile has a similar q_a dependence to the calculated location of the strike points, demonstrating the fact that the edge island intersects the LFS limiter. Experiments on DIII-D

and MAST have observed the evidences of strike points on the target plate using V_f as the indicators [34, 35].

4. Dynamics of edge plasma profiles during the opening of edge islands

4.1. q_a-dependence

In order to investigate the influence of magnetic topology on plasma transport properties during the opening of the edge magnetic island, a series of discharges with different q_a has been performed on the J-TEXT with the first RMP configuration as shown in table 1. In this experiment, q_a is
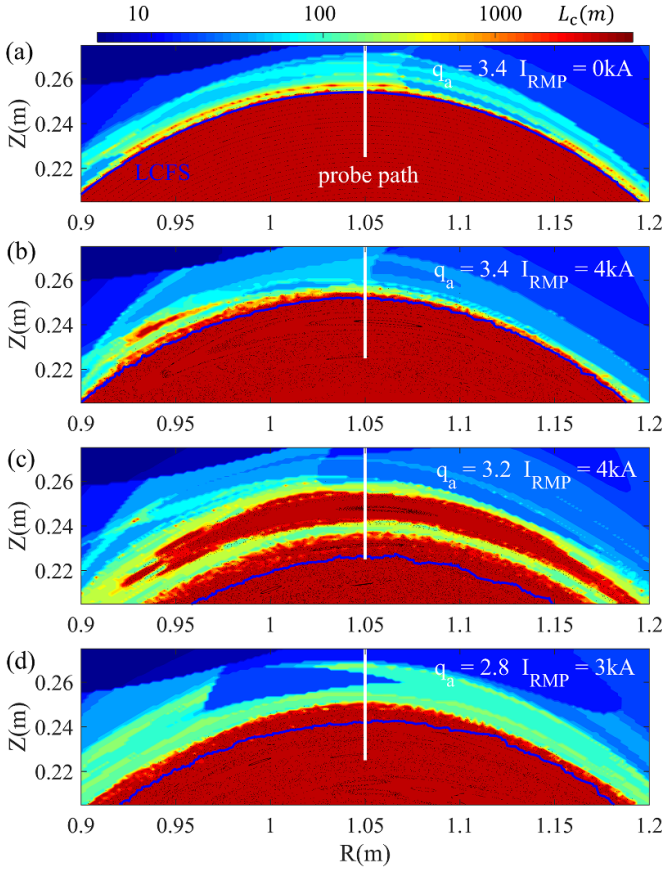
Figure 6. The connection length L_c (R, Z) for four cases with (*a*) $q_a = 3.4$ and $I_{RMP} = 0$kA, (*b*) $q_a = 3.4$ and $I_{RMP} = 4$kA, (*c*) $q_a = 3.2$ and $I_{RMP} = 4$kA and (*d*) $q_a = 2.8$ and $I_{RMP} = 3$kA. The connection length is marked by different colors (in unit of meter on a logarithmic scale). The real parameter settings used in the calculation of L_c (R, Z) are from discharges 1056 890, 1056 894, 1056 901 and 1056 903. The white line indicates the Langmuir probe path and the blue curve indicates the LCFS.

decreased in each discharge by increasing the plasma current I_p while maintaining other plasma parameters almost constant.

Figure 6 depicts the 2D distributions of the field-line connection length L_c (R, Z) in the RLP poloidal plane, calculated based on the HINT equilibrium for four discharges with different combinations of q_a (3.4, 3.4, 3.2 and 2.8) and RMP current I_{RMP} (0 kA, 4 kA, 4 kA and 3 kA), respectively. The L_c is plotted on a logarithmic scale from 0 m to 5000 m. The radial position of the LCFS for the reference plasma configuration ($q_a = 3.4$ and $I_{RMP} = 0$kA) is $Z \sim 0.255$ m at $R = 1.05$ m. A comparison of figures 6(*b*)–(*d*) reveals that the edge $m/n = 3/1$ magnetic island gradually moves outward, transitioning from a closed island inside the LCFS ($q_a = 3.4$) to a partially open island in the SOL ($q_a = 3.2$) and finally to a fully open island in the SOL ($q_a = 2.8$). For the case with $q_a = 3.4$, a magnetic island with a width of ~ 2.0 cm is positioned at $Z \sim 0.242$ m, very close to the LCFS. The LCFS of the target plasma is defined herein as the radial position at

which L_c reaches inward to infinity. For the case with $q_a = 3.2$, the island is pushed outward to intersect the local limiter, resulting in a remnant magnetic island with a width of ~ 1.0 cm located at $Z \sim 0.250$ m between the LCFS of the confined plasma and limiter. The remnant island is the uncut part of the magnetic island (a closed region with infinite L_c). In this case, the edge topology becomes very similar to the island divertor configuration performed in W7-X [36] and LHD [37]. The L_c drops to a finite value at the inner boundary of the island, creating a visible gap of ~ 1.0 cm at $Z \sim 0.240$ m between the remnant island and LCFS, which moves inward to $Z \sim 0.228$ m at $R = 1.05$ m. As q_a decreases further to 2.8, the island is cut by the limiter by more than half, resulting in a fully opened magnetic island structure with no remnant island in the SOL. The LCFS shifts to $Z \sim 0.243$ m at $R = 1.05$ m, and an open magnetic field region with L_c longer than 1000 m is predicted between the LCFS and the radial position of the limiter.

As indicated (the white line) in figure 6, the RLP plunges through the O-point of the magnetic island. For these different discharges, the corresponding L_c along the RLP path has been plotted in figure 7(*f*). The radial profiles of electron temperature T_e, density n_e, pressure P_e, floating potential V_f and radial electric field E_r are also shown figures 7(*a*)–(*e*). In addition, the four limiter's radial positions are indicated by the arrows in figure 7(*f*): black for the LFS and bottom limiters, blue for the HFS limiter and red for the top limiter.

It is clear that the T_e, n_e and P_e are significantly reduced in both cases of closed island and partially open islands compared to the non-RMP reference case. In the $q_a = 3.4$ case, a flattening of P_e profile is observed between 0.234 m $< Z < 0.250$ m, where the magnetic island is located (see figure 6(*b*)). However, in this region, the value of T_e varies between 28 and 35 eV and n_e shows a small peak at $Z \sim 0.245$ m, indicating that no flattening is observed in T_e and n_e profiles inside the magnetic island. For the $q_a = 3.2$ case, the flat P_e region shifts outward, and a narrower flat P_e region along with lower P_e is observed at 0.245 m $< Z < 0.254$ m. This corresponds to the fact that the magnetic island moves outward and the island becomes smaller due to being cut. The gap between the LCFS and remnant island is characterized by steep slopes of the T_e, n_e and P_e profiles. This occurs because the L_c in this gap is significantly longer than the electron mean free path λ_e, thus helping to maintain the gradients [38]. At the edge region of J-TEXT, the electron mean free path $\lambda_e = \sqrt{\frac{T_e}{m_e}} \frac{12\pi^{3/2}}{\sqrt{2}} \frac{\varepsilon_0^2 m_e^{1/2} T_e^{3/2}}{n_i Z_i^2 e^4 \ln \Lambda}$ [38] is calculated to be about 10 m assuming that $n_i = n_e$. For the $q_a = 2.8$ case, the n_e profile of the measured region appears to be unaffected when compared to the non-RMP case. While different T_e and P_e profiles are observed, with steep slopes in the region of 0.250 m $< Z < 0.260$ m where L_c is ~ 100 m and steeper slopes radially inwards at $Z < 0.250$ m where L_c further increases to ~ 1000 m.

The experimental profiles of V_f and E_r are also greatly impacted by the changes in magnetic topology. In the case of $q_a = 3.4$, V_f shows a similar distribution to the reference case at the SOL region of $Z > 0.255$ m, but changes to a small
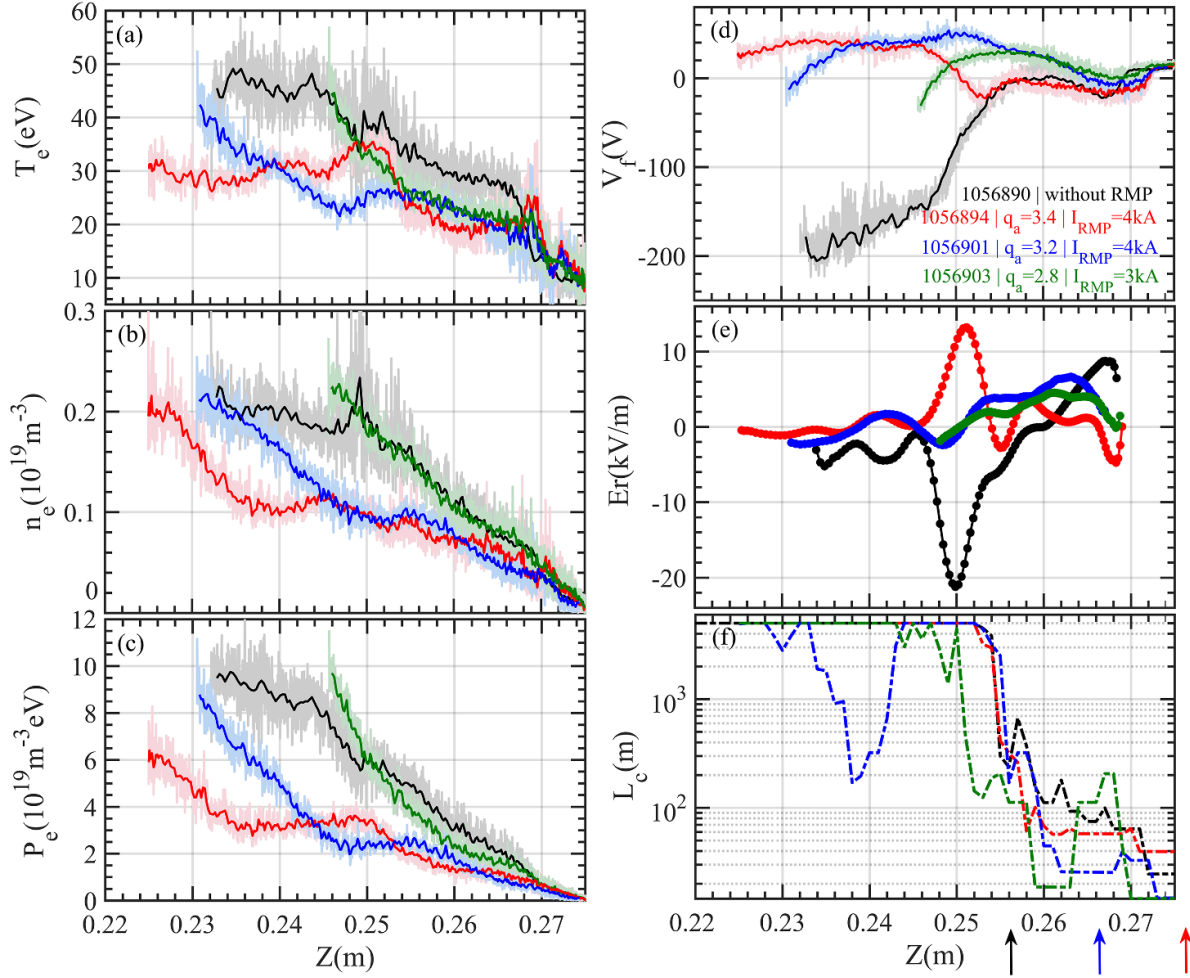
Figure 7. Radial profiles in the experiments of q_a-dependence of (*a*) electron temperature T_e, (*b*) electron density n_e, (*c*) electron pressure P_e, (*d*) floating potential V_f, (*e*) radial electric field E_r and (*f*) the connection length L_c along the probe path. The radial radius of four limiters are indicated by arrows: LFS and bottom (black arrow), HFS (blue arrow) and top (red arrow). The shaded regions in (*a*)–(*d*) denote the standard deviation of the measurements.

positive value inside the magnetic island. For the $q_a = 3.2$ and 2.8 cases, V_f exhibit small positive values inside the remnant island and the SOL region with $L_c < 1000$ m, then shift to negative values at the region with $L_c > 1000$ m. The changes in V_f and T_e lead to alterations in the E_r profile. In the reference case, a negative E_r well is observed at the edge region $Z \sim 0.250$ m, as documented in many tokamak devices. For the other three cases with RMP, E_r signals develop from large negative towards small negative and even positive when compared to the non-RMP reference case. For the case of $q_a = 3.4$, E_r signal reverses from positive to negative across the island, as has been observed in many devices, such as LHD [39] and KSTAR [10]. Near $Z = 0.250$ m, E_r develops towards a large positive value, even up to 12 kV m^{-1}, which may be due to the stochastization at the outer boundary of the magnetic island. For the $q_a = 3.2$ case, a negative E_r well is observed inside the remnant island. Radially inward, E_r signal develops to positive at $Z \sim 0.240$ m and further inverses to negative again at $Z \sim 0.235$ m. These results indicate that the electrons are well confined in the remnant island with infinite L_c and open

regions with $L_c > 1000$ m, but are more easily lost than ions to the limiters/vessel along the open magnetic fields in the open region with $L_c < 1000$ m. Similar result can be observed for the $q_a = 2.8$ case, the E_r signal changes from positive to negative at $Z \sim 0.250$ m, where L_c increases from 200 m to over 1000 m.

4.2. RMP configuration-dependence

The impact of different magnetic configurations on edge transport with $q_a = 3.2$ and $I_{RMP} = 4$kA are also investigated by altering the polarity of RMP coil currents. The edge islands induced by different RMP configurations face different limiters (see figures 1(*c*) and (*d*)), leading to different intersection patterns between the magnetic island and the poloidally localized limiter, thus different 3D boundary structure. Similarly, figure 8 presents the modeled connection length distribution L_c (R, Z) in the poloidal plane of RLP for the first and second configurations described in table 1. Compared with the first RMP configuration, the plasma boundary Poincaré plot of
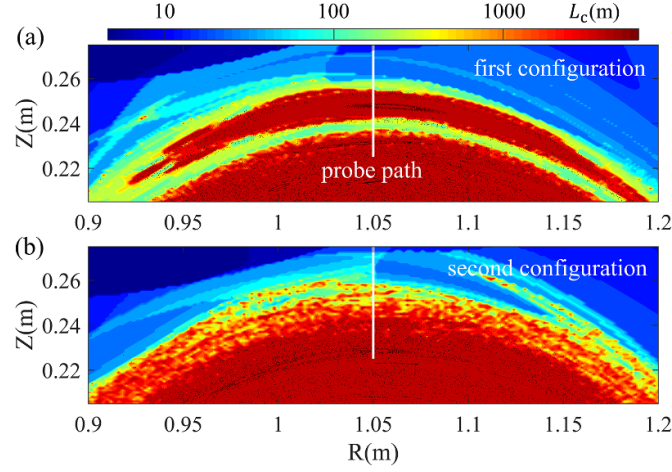
Figure 8. The connection length L_c (R, Z) for two cases with (*a*) the first magnetic configuration and (*b*) the second magnetic configuration. The connection length is marked by different colors (in unit of meter on a logarithmic scale). The real parameter settings used in the calculation of L_c (R, Z) are from discharges 1056 901 and 1056 898. The white line indicates the Langmuir probe path.
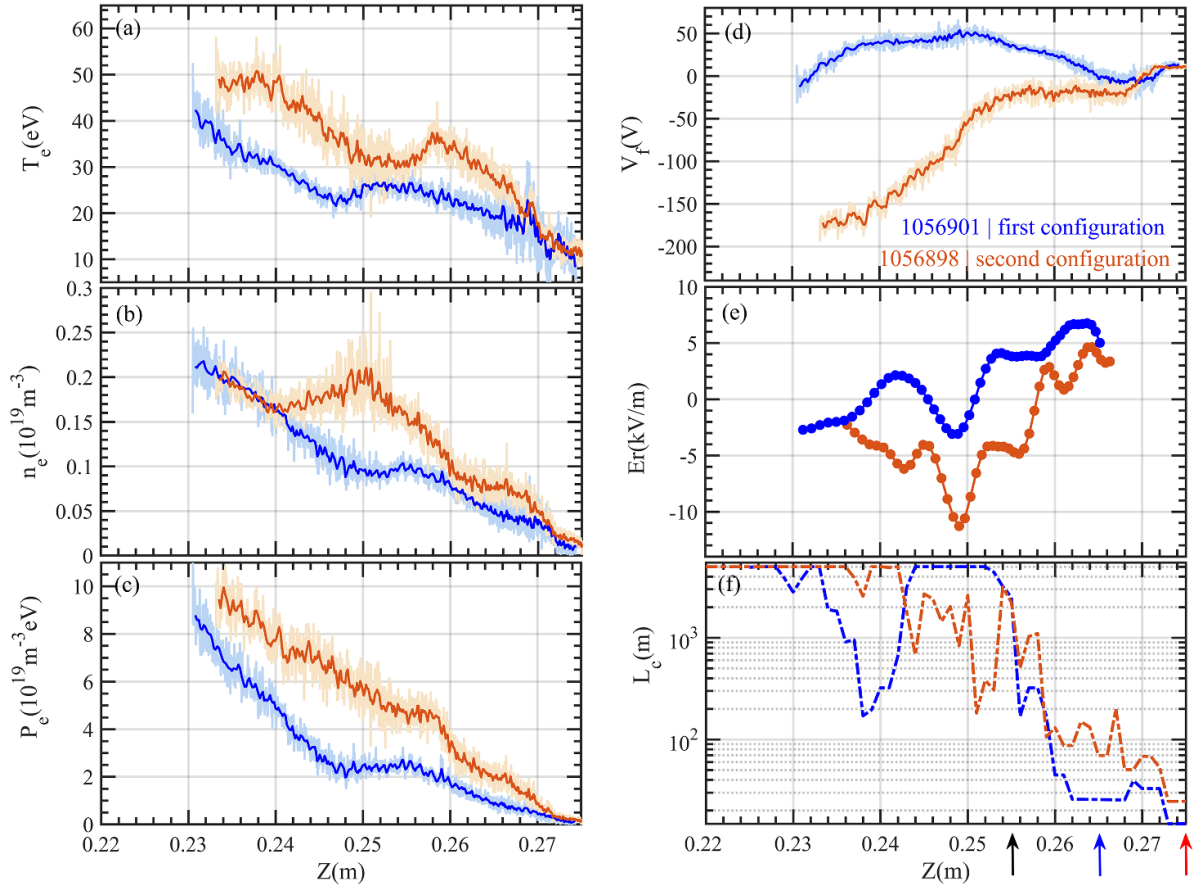

Figure 9. Radial profiles in the experiments of RMP configuration-dependence of (*a*) electron temperature T_e, (*b*) electron density n_e, (*c*) electron pressure P_e, (*d*) floating potential V_f, (*e*) radial electric field E_r and (*f*) the connection length L_c along the probe path. The radial radius of four limiters are indicated by arrows: LFS and bottom (black arrow), HFS (blue arrow) and top (red arrow).

the second RMP configuration shows stronger stochastization and no obvious remnant islands in the SOL region. However, the connection length L_c in most regions is very long compared with the electron mean free path λ_e. The RLP plunges through different island phases, i.e. near O-point for the first RMP configuration and X-point for the second RMP configuration. Figure 9 shows the measured edge profiles of T_e, n_e and P_e, V_f, E_r and the calculated L_c along the RLP path corresponding to these two RMP configurations, respectively. The increases in T_e, n_e and P_e are observed in most regions with
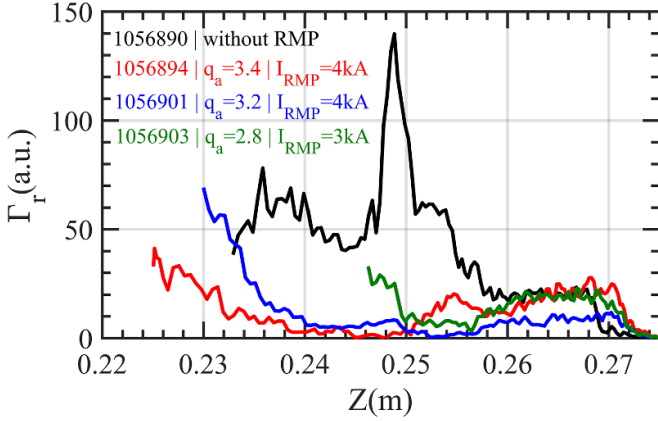
Figure 10. The radial profiles of fluctuation-driven particle flux Γ_r in the experiments of q_a-dependence.

the second RMP configuration compared to the first RMP configuration. And there is no obvious flattening in the P_e profile, which is consistent with the prediction of pressure profile near the X-point. The P_e profile exhibits two rapid increases at $Z \sim 0.270$ m and 0.260 m, where the connection length L_c expands from ~ 20 m to 100 m and further to ~ 1000 m. Furthermore, the V_f profile measured for the second RMP configuration shows a large negative value from the plasma edge to the plasma core. And the E_r profile changes from the positive to the negative at $Z \sim 0.260$ m, again demonstrating the fact that the electrons are well confined when the $L_c \gg \lambda_e$.

4.3. Turbulence-driven particle flux

In the experiments of q_a-dependence, the opening of the edge $m/n = 3/1$ magnetic island leads to a significant reduction in the edge T_e, n_e and P_e profiles. These reductions persist until the island is cut by more than half (absence of closed remnant island), indicating that the presence of an edge closed/ remnant magnetic island has an enhanced effect on both the heat and particle transport at the plasma edge. It should be noted that during this process, the plasma volume alters proportionally due to the shift of the LCFS. The edge fluctuation-driven particle flux Γ_r, as depicted in figure 10, is also affected by the edge magnetic topology. Here, Γ_r is calculated from the fluctuating density $\tilde{n}_e$ and poloidal electric field $\tilde{E}_\theta$ by $\Gamma_r = \tilde{n}_e \tilde{E}_\theta / B_t \sim \tilde{I}_s \tilde{E}_\theta / B_t$ when neglecting the temperature fluctuation $\tilde{T}_e$. $\tilde{E}_\theta$ is measured by two poloidally separated tips (tip 6 and tip 8 in figure 2(*b*)) with $d = 7$ mm by $\tilde{E}_\theta = \left(\tilde{V}_{f2} - \tilde{V}_{f1} \right) / d$. It is apparent that Γ_r experiences a significant reduction in the outward radial direction (>0) inside the edge closed/remnant magnetic islands due to the absence of pressure gradients. Since turbulence contributes largely to the edge cross-transport in fusion devices, a decrease in Γ_r is expected to result in reduced heat and particle transport. This result suggests that the radial projection of the parallel transport along the field lines located around the islands/stochastic zones can provide a mechanism to effectively enhance plasma radial transport [40]. For the fully open island case, the Γ_r is reduced within the

region of 0.250 m $< Z < 0.260$ m with a possible interpretation of a local depression by the $E_r \times B$ shear. In the region of $Z < 0.250$ m, the Γ_r is not deeply measured but begins to increase due to the large pressure gradient.

5. Discussion and conclusion

In this contribution, the direct experimental evidence on the J-TEXT tokamak has shown the dynamic of edge magnetic topology during the opening of edge island. The discharge with an $m/n = 3/1$ edge magnetic island induced by RMP has been performed, in which the plasma current is ramped up to push the $q = 3$ rational surface outwards. The intersections between the edge island and poloidally localized limiter are experimentally confirmed by the limiter Langmuir probe measurements, and the HINT-predicted strike points generated by the intersections are in qualitative agreement with the negative floating potential pattern.

The effects of the magnetic topology on the edge plasma profiles have also investigated. The radial profiles of electron temperature T_e, density n_e, pressure P_e and radial electric field E_r are obtained from the Langmuir probe. A series of q_a-dependence experiments are carried out to investigate the edge plasma profile dynamics during the opening of edge magnetic island. Three different edge magnetic structures, including edge closed magnetic island, partially open island with remnant magnetic island and fully open island without remnant island, are compared with the reference case without RMP. In the intermediate case, the connection length L_c is infinite inside the remnant island but becomes a finite value at the gap between the remnant island and the LCFS. Flat P_e but non-flat T_e and n_e profiles are observed inside the remnant magnetic islands, similar to the observations in edge closed magnetic island. The local flat P_e profile is shifted outwards accompanied by a narrower flattened P_e region when transitioning the edge closed island to the partially open island. In the latter case, n_e and P_e at the core are observed to be increased, which is correlated with the large pressure gradient at the edge.

Additionally, two magnetic configurations induced by different RMP polarities are compared as well. The Langmuir probe plunges through the O-point in one configuration but through the X-point in another configuration. In the latter configuration, T_e, n_e and P_e are observed to increase, with a maximum n_e and a minimum T_e at $Z \sim 0.250$ m. Simulation with EMC3-EIRENE code shows that the radiation pattern is peaked around the X-point of the magnetic island [41]. This could be a possible interpretation for the maximum n_e and minimum T_e. But we also need to note that the separatrix of the magnetic island gains in stochastization in the latter RMP configuration, i.e. the X-point of the island is eroded.

Finally, some common features are observed in these different edge magnetic structures. The steep slopes of the T_e, n_e and P_e profiles are observed in the SOL regions with long L_c, and the longer L_c, the steeper slope. E_r is characterized by a negative well inside the remnant island with infinite L_c and in the SOL with $L_c > 1000$m but by a positive value in

the SOL with $L_c < 1000$m, indicating that the electrons are well confined when $L_c \gg \lambda_e$ but lost much faster than the ions along the open magnetic field lines with relatively short L_c. The turbulence-driven particle flux Γ_r is also measured by the Langmuir probe. Γ_r inside the remnant island is small whereas much larger in the SOL.

Acknowledgments

ORCID iDs

Y. Liang ⓘ https://orcid.org/0000-0002-9483-6911
N.C. Wang ⓘ https://orcid.org/0000-0001-6797-2398
S. Zhou ⓘ https://orcid.org/0000-0002-1407-0574
Z.P. Chen ⓘ https://orcid.org/0000-0002-8330-0070
Z.H. Jiang ⓘ https://orcid.org/0000-0002-4971-080X
Z.Y. Chen ⓘ https://orcid.org/0000-0002-8934-0364
P. Drews ⓘ https://orcid.org/0000-0002-6567-1601
A. Knieps ⓘ https://orcid.org/0000-0003-0083-7188
S. Xu ⓘ https://orcid.org/0000-0002-0033-3468
J.W. Liu ⓘ https://orcid.org/0000-0003-1324-5659

References

[1] König R. *et al* 2002 *Plasma Phys. Control. Fusion* **44** 2365
[2] Liang Y. *et al* 2007 *Phys. Rev. Lett.* **98** 265004
[3] Finken K.H. *et al* 2007 *Phys. Rev. Lett.* **98** 065001
[4] Jakubowski M.W. *et al* 2006 *Phys. Rev. Lett.* **96** 035004
[5] Fitzpatrick R. 1995 *Phys. Plasmas* **2** 15
[6] Günter S., Gude A., Maraschek M. and Yu Q. (ASDEX Upgrade Team) *Plasma Phys. Control. Fusion* 1999 **41** 767
[7] Hender T.C. *et al* 1992 *Nucl. Fusion* **32** 2091
[8] Spakman G.W. *et al* 2008 *Nucl. Fusion* **48** 115005
[9] Hegna C.C. and Callen J.D. 1992 *Phys. Fluids B* **4** 4072
[10] Choi M.J. *et al* 2017 *Nucl. Fusion* **57** 126058
[11] Choi M.J. 2021 *Rev. Mod. Plasma Phys.* **5** 9
[12] Finken K.H. *et al* 2004 *Plasma Phys. Control. Fusion* **46** B143
[13] Evans T.E. *et al* 2005 *J. Nucl. Mater.* **337–339** 691
[14] McCool S.C. *et al* 1989 *Nucl. Fusion* **29** 547
[15] Dong C., Morita S., Kobayashi M., Goto M., Masuzaki S., Morisaki T. and Wang E. 2011 *Phys. Plasmas* **18** 082511
[16] Schmitz O. *et al* 2008 *Nucl. Fusion* **48** 024009
[17] Park G., Chang C.S., Joseph I. and Moyer R.A. 2010 *Phys. Plasmas* **17** 102503
[18] Xu Y. *et al* 2007 *Nucl. Fusion* **47** 1696
[19] Suzuki Y. *et al* 2016 *Nucl. Fusion* **56** 092002
[20] Schmitz O., Evans T.E., Fenstermacher M.E., Lanctot M.J., Lasnier C.L., Mordijck S., Moyer R.A. and Reimerdes H. 2014 *Nucl. Fusion* **54** 012001
[21] Hu Q. *et al* 2016 *Nucl. Fusion* **56** 092009
[22] Wang N. *et al* 2014 *Nucl. Fusion* **54** 064014
[23] Yan W. *et al* 2018 *Plasma Phys. Control. Fusion* **60** 035007
[24] Zhang X. *et al* 2021 *Plasma Sci. Technol.* **23** 125101
[25] Zhuang G. *et al* 2011 *Nucl. Fusion* **51** 094020
[26] Rao B. *et al* 2014 *Fusion Eng. Des.* **89** 378
[27] Liang Y. *et al* 2019 *Nucl. Fusion* **59** 112016
[28] Suzuki Y. 2017 *Plasma Phys. Control. Fusion* **59** 054008
[29] Yang J., Chen Z., Liu H., Wang T., Zhu M., Song Z., Wang Z., Zhuang G. and Ding Y. 2019 *Plasma Sci. Technol.* **21** 105105
[30] Yang Z.J., Pan X.M., Ma X.D., Ruan B.W., Zhou R.B. and Zhang C. 2016 *Rev. Sci. Instrum.* **87** 11E112
[31] Zhang X.L. *et al* 2019 *Fusion Eng. Des.* **147** 111241
[32] Stangeby P.C. 2000 *The Plasma Boundary of Magnetic Fusion Devices* (Institute of Physics Publishing)
[33] Harting D.M., Liang Y., Jachmich S., Koslowski R., Arnoux G., Devaux S., Eich T., Nardon E., Reiter D. and Thomsen H. 2012 *Nucl. Fusion* **52** 054009
[34] Orlov D.M., Moyer R.A., Evans T.E., Wingen A., Buttery R.J., Ferraro N.M., Grierson B.A., Eldon D., Watkins J.G. and Nazikian R. 2014 *Nucl. Fusion* **54** 093008
[35] Cahyna P., Peterka M., Kirk A., Thornton A., Harrison J., Muir D. and Panek R. 2013 *J. Nucl. Mater.* **438** S326
[36] Strumberger E. 1996 *Nucl. Fusion* **36** 891
[37] Morisaki T. *et al* 2005 *J. Nucl. Mater.* **337–339** 154
[38] Wesson J. and Campbell D.J. 2011 *Tokamaks* (Oxford University Press)
[39] Ida K. *et al* 2001 *Phys. Rev. Lett.* **88** 015002
[40] Kobayashi M. *et al* 2015 *Nucl. Fusion* **55** 104021
[41] Feng Y. *et al* 2005 *Nucl. Fusion* **45** 89